IEEE Access
Multidisciplinary ⋮ Rapid Review ⋮ Open Access Journal

Received July 8, 2019, accepted August 19, 2019, date of publication August 29, 2019, date of current version September 17, 2019.

Digital Object Identifier 10.1109/ACCESS.2019.2938267

Control of Diabetes Mellitus by Advanced Robust Control Solution

LEVENTE KOVÁCS[1], (Senior Member, IEEE), GYÖRGY EIGNER[1], (Senior Member, IEEE), MÁTÉ SIKET[1], AND LÁSZLÓ BARKAI[2,3]

[1]Physiological Controls Research Center, Research, Innovation and Service Center, Óbuda University, H-1034 Budapest, Hungary
[2]Department of Paediatrics and Adolescent Medicine, Faculty of Medicine, Pavol Jozef Šafárik University in Košice, 040 11 Košice, Slovakia
[3]Faculty of Health Care, Institute of Theoretical Health Sciences, University of Miskolc, 3515 Miskolc, Hungary

Corresponding author: György Eigner (eigner.gyorgy@nik.uni-obuda.hu)

This project has received funding from the European Research Council (ERC) under the European Union's Horizon 2020 Research and Innovation Programme (grant agreement No 679681) and the Hungarian Diabetes Association.

ABSTRACT The current article investigates the possibilities of designing a robust control solution for a control problem related to type 1 diabetes mellitus. The proposed control methodology exploits linear parameter varying, linear matrix inequality, tensor product model transformation and extended Kalman filtering, four advanced control methods in order to guarantee hard safety control constraints for diabetic patients. In this research we have applied an extension of the minimal model to simulate the glucose-insulin dynamics and the glucose and insulin absorption of a diabetic patient. We have validated our results on numerical simulations by using realistic patient data. During the evaluation we have used randomized glucose intakes both in time and amount (as ''unfavorable'' disturbance signals). Furthermore, we did a long-term (30 days) assessment to confirm the stability of the proposed framework. The results have shown that the developed controller effectively intervenes into the process and provides appropriate control action by avoiding hypoglycemia thereby satisfying the predefined quantity and quality requirements.

INDEX TERMS Extended Kalman filter, linear matrix inequality, linear parameter varying-based control, tensor product model transformation, type 1 diabetes mellitus.

I. INTRODUCTION

Nowadays the application of advanced physiological modeling and control have crucial importance in biomedical engineering [1]. There are many fields in which these solutions can be found in use. Examples include the regulation of anesthesia [2], control of blood glucose (BG) level of patients suffering from diabetes mellitus (DM), i.e., the Artificial Pancreas (AP) problem [3], [4] and the regulation of tumor growth [5]. In case of DM, many challenging aspects occur which have to be kept in mind during the development of solutions for treatment.

On the one hand, several types of DMs exist which have their own specificities and dependencies. The most frequently occurring types are the Type 1 DM (T1DM), Type 2 DM (T2DM) and Gestational DM (GDM) [6]. The common point among these types of DMs is the malfunction of the metabolic system related to the insulin hormone, more precisely, the lack of insulin (T1DM) or the decreasing effectivity of it (T2DM, GDM) [7].

On the other hand, all of them require unique approaches from biomedical engineering point of view: the applicable modeling and control techniques are similar, but varying according to the needs. Due to the nature of the problem, the applicable models are highly nonlinear, there are parameter uncertainties which may vary over time, the parameter sets are patient dependent, time delay affects can occurr, etc. Nevertheless, one thing is common in all cases: the primary goal of the control is to keep the BG level in a healthy range without high variabilities in its value over time, focusing primarily to hypoglycemia avoidance. [8]–[10].

In this research we investigate the AP context focusing on T1DM – where the β-cells of the pancreas lost their ability to produce insulin hormone. Without insulin, the glucose dependent cells are not able to absorb glucose molecules from the blood through the insulin dependent gates located in the cellular wall of the cells [11]. Thus, without external insulin intake in short-term and appropriate insulin therapy in

The associate editor coordinating the review of this manuscript and approving it for publication was Zehong Cao.

long-term the patients will face serious health consequences, including death [6].

Appropriate treatment both from quality and quantity point of view can be realize only by using advanced control solutions [12]. However, the aforementioned conditions have to be solved by the used methods. Different solutions exist for AP, although all of them have their own limitations [3]: the personalization and the generalization are antonyms, but both of them have to be taken into account during the development. The most frequently used methods – which also have been patented recently as closed loop DM therapies – is the model predictive control (MPC), proportional-integral-derivative (PID) control and fuzzy logic based ideas. Clinical trials have been done to investigate the effectivity of these methods [13]–[18]. In these cases, we have to accept the validity of the model and need to deal with the constraints caused by the approximations. There are several challenges needed to be dealt with regarding the aforementioned control methodologies. For example the sensor delay (mainly caused by the applied sensor technology due to phenomenological, modeling, manufacturing, or software related issues [19]), delayed insulin effect (due to the absorption, diffusion, degradation of synthetic insulin [20]), or even overnight supervision, which is also a challenge due to the lack of food intake [15], [21]. These effects and circumstances may lead to overdosing the insulin during automated treatment. With single hormone control – when the only action possible in case of overdosing is to turn off the insulin pump – these are critical issues [21]–[24].

Robust control approaches can be alternatives to the above mentioned control opportunities, where the aims could be to develop robust solution from parameter, model, external excitations, or other points of view. An applicable method is the fixed point based controller design (RFPT). In case of RFPT theorem the control goal is transformed into a fixed point problem which is solved via iterations during the control action. This adapting property allows the use of highly approximated model of the process to be controlled and we do not need to know information about the internal states of the system (the human body in this case) [25], [26].

It has been also proven that the robust control techniques can be useful regarding the control of DM, since they are able to deal with many kind of uncertainties coming from both the patient and system side. In general, the goal of the application with them was to provide acceptable control action from the system point of view (total avoidance of hypoglycemia, limited control signal, etc.) and not to provide the ''best one'' (the most optimal one) [4], [27], [28].

In the recent years, linear parameter varying (LPV) based controller design methods have came to the fore due to their beneficial properties. This modeling technology can be combined with linear matrix inequality (LMI) based optimization which guarantees the robust stability and satisfies the performance of LPV control system via gain-scheduling in real time. Furthermore, it achieves this by using the measured or estimated parameters [29]–[32]. Among other techniques, the tensor product (TP) model transformation is another attractive possibility, since it can be easily combined with LMI based design on given LPV models and because of its strong ability in manipulating the convex hull in polytopic forms. By combining the TP framework with parallel distributed compensation (PDC) [33] controller design, the TP-based LMI controller is able to provide the stability of the system – regardless the variation of the parameter vector in time [34]–[45].

In this paper we proposed a TP-LMI-LPV based controller design method for T1DM. The paper is structured as follows. First, we introduce the applied T1DM model and its LPV based control oriented form. After, we present the TP model transformation and the realized TP model. Hereupon, we demonstrate the LMI design technique. Afterwards, the design of the extended Kalman filtering (EKF) is presented followed by the finalized control structure and the results of our numerical simulations. In the discussion section we analyzed the results. Finally, we have concluded our work and presented the directions of our future research.

II. MODEL DESCRIPTION AND PROBLEM DECLARATION

A. MODEL DESCRIPTION

The applied model consists of different submodels: core model to describe the glucose-insulin dynamics [46]; carbohydrate (CHO) absorption submodel [47]; and insulin absorption submodel [47]. The application of mixed models are frequent in the scientific literature [48]–[50]. The CHO and insulin sub-models have been proposed by Hovorka et al. originally in [47], [51]. Both sub-models are two compartmental models. The CHO submodel describes how the orally ingested CHO affects the rate of appearance of glucose in the blood. The insulin absorption submodel describes the rate of appearance of insulin in the blood injected subcutaneously. The submodels are represented by (1a) - (1d). The core model – first published in [46] – is responsible for describing the glucose-insulin dynamics (1e) - (1g).

$$\dot{D}_1(t) = -\frac{1}{\tau_D}D_1(t) + \frac{1000A_g}{M_{wG}V_G}C \cdot d(t) \tag{1a}$$

$$\dot{D}_2(t) = -\frac{1}{\tau_D}D_2(t) + \frac{1}{\tau_D}D_1(t) \tag{1b}$$

$$\dot{S}_1(t) = -\frac{1}{\tau_S}S_1(t) + \frac{1}{V_I}u(t) \tag{1c}$$

$$\dot{S}_2(t) = -\frac{1}{\tau_S}S_2(t) + \frac{1}{\tau_S}S_1(t) \tag{1d}$$

$$\dot{G}(t) = -(p_1 + X(t))G(t) + p_1G_B + \frac{1}{\tau_D}D_2(t) \tag{1e}$$

$$\dot{X}(t) = -p_2X(t) + p_3(I(t) - I_B) \tag{1f}$$

$$\dot{I}(t) = -n(I(t) - I_B) + \frac{1}{\tau_S}S_2(t) \tag{1g}$$

The core model has three state variables, which are connected to the blood plasma, these are the following: $G(t)$ [mg/dL], the blood glucose (BG) concentration,

$X(t)$ [1/min], insulin-excitable tissue glucose uptake activity and $I(t)$ [mU/L], the blood insulin concentration. The glucose and insulin absorption submodels consist of the $D_1(t)$ [mg/dL], $D_2(t)$ [mg/dL], $S_1(t)$ [mU/L] and $S_2(t)$ [mU/L], respectively. The disturbance input $d(t)$ [g/min] represents the glucose intake which is transformed by the $\big((1000\,A_g)/(M_{wG}V_G)\big)C$ complex into the appropriate dimension to fit to the $D_1(t)$. The control input $u(t)$ [mU/L/min] is directly connected to the $S_1(t)$. The detailed description of the used model parameters can be found in Table 1.

TABLE 1. The applied parameters of the models [46], [47].

Notation	Value	Unit	Description
G_B	110	[mg/dL]	Basal glucose level
I_B	1.5	[mU/L]	Basal insulin level
p_1	0.028	[1/min]	Transfer rate
p_2	0.025	[1/min]	Transfer rate
p_3	0.00013	[L/(mU min)]	Transfer rate
n	0.23	[1/min]	Time constant for insulin disappearance
BW	75	[kg]	Body weight
V_I	0.12 BW	[L]	Insulin distribution volume
V_G	0.16 BW	[L]	Glucose distribution volume
M_{wG}	180.1558	[g/mol]	Molecular weight of glucose
A_g	0.8	-	Glucose utilization
C	18.018	[mmol/L]	Convert rate between [mg/dL] and [mmol/L]
τ_D	40	[min]	CHO to glucose absorption constant
τ_S	55	[min]	Insulin absorption constant

B. CONTINUOUS GLUCOSE MONITORING SYSTEM MODEL DESCRIPTION

Modeling the sensor noise in continuous glucose monitoring system (CGMS) applications is a crucial question. CGMS devices measure the BG level from the subcutaneous space in the arm. However, the measured values can be different from a given average BG level in the body. There are different effects which may make the measurements corrupt such as the time delay, heat effects an so on. These may lead to sensor decalibration. In order to model these phenomena we have applied the CGMS model of [52]. The developed model can be directly connected to the introduced model described by (1e) - (1g).

$$e_k = 0.7(e_{k-1} + v_k), \quad k \geq 1, \tag{2}$$

$$v_k \sim N_{iid}(0, 1), \tag{3}$$

$$\eta_k = \xi + \lambda \sinh\left(\frac{e_k - \gamma}{\delta}\right), \tag{4}$$

$$\dot{G}_{sub}(t) = \frac{1}{\tau_{sub}}(G(t) - G_{sub}(t)), \tag{5}$$

$$G_{CGM}(kT) = G_{sub}(kT) + \eta_k. \tag{6}$$

We used the parameters given by [52]: τ_{sub}=15 min, ξ=-5.471 mg/dL, λ=15.96 mg/dL, γ=-0.5444 and δ=1.6898. The Brownian motion like term can be initialized with $e_0 \sim N_{iid}(0, 1)$. The noisy measurement data can be calculated by using the sampled output of the virtual patient system $G(t)$. The model includes a first order process in order to approximate the delay between the different glucose compartments and a noise term with Johnson-like distribution.

C. AIM OF THE CONTROL

Our research aim is to hold the blood glucose level – described by $G(t)$ – within a given determined range. Due to physiological limitations, our primary goal is to avoid hypoglycemia and allow only short hyperglycemic periods. The selected constraint in this research was: 60 [mg/dL] (3.33 [mmol/L]) $\leq G(t) \leq$ 320 [mg/dL] (17.76 [mmol/L]) which shall not be exceeded by the blood glucose level at all.

III. TENSOR PRODUCT MODEL TRANSFORMATION OF THE LPV MODEL

A control engineering summary is given in the following to briefly describe and highlight the applied modeling and control methods.

A. LPV MODEL FORM

Consider the following nonlinear time-varying system in state space form [53], [54]:

$$\begin{aligned}
\dot{\mathbf{x}}(t) &= \mathbf{A}(t)\mathbf{x}(t) + \mathbf{B}(t)\mathbf{u}(t) + \mathbf{E}(t)\mathbf{d}(t) \\
\mathbf{y}(t) &= \mathbf{C}(t)\mathbf{x}(t) + \mathbf{D}(t)\mathbf{u}(t) + \mathbf{D}_2(t)\mathbf{d}(t) \\
\begin{pmatrix}\dot{\mathbf{x}}(t)\\ \mathbf{y}(t)\end{pmatrix} &= \mathbf{S}(t)\begin{pmatrix}\mathbf{x}(t)\\ \mathbf{u}(t)\\ \mathbf{d}(t)\end{pmatrix} \\
\mathbf{S}(t) &= \begin{bmatrix}\mathbf{A}(t) & \mathbf{B}(t) & \mathbf{E}(t)\\ \mathbf{C}(t) & \mathbf{D}(t) & \mathbf{D}_2(t)\end{bmatrix},
\end{aligned} \tag{7}$$

where $\mathbf{x}(t) \in \mathbb{R}^n$, $\mathbf{y}(t) \in \mathbb{R}^k$, $\mathbf{u}(t) \in \mathbb{R}^m$ and $\mathbf{d}(t) \in \mathbb{R}^l$ are the state-, output-, control input- and disturbance input-vectors, respectively. The $\mathbf{A}(t) \in \mathbb{R}^{n\times n}$ is the state matrix, $\mathbf{B}(t) \in \mathbb{R}^{n\times m}$ is the control input matrix, $\mathbf{E}(t) \in \mathbb{R}^{n\times l}$ is the disturbance input matrix, $\mathbf{C}(t) \in \mathbb{R}^{k\times n}$ is the output matrix, $\mathbf{D}(t) \in \mathbb{R}^{k\times m}$ is the control feed-forward matrix, $\mathbf{D}_2(t) \in \mathbb{R}^{k\times l}$ is the disturbance feed-forward matrix. The $\mathbf{S}(t) \in \mathbb{R}^{(n+k)\times(n+m+l)}$ is the so-called system matrix.

Assume that the nonlinearity-causing terms of the model are selected as scheduling variables $p_i(t)$. Therefore, the (7) can be described as an LPV system in the following way [53], [55]:

$$\begin{aligned}
\dot{\mathbf{x}}(t) &= \mathbf{A}(\mathbf{p}(t))\mathbf{x}(t) + \mathbf{B}(\mathbf{p}(t))\mathbf{u}(t) + \mathbf{E}(\mathbf{p}(t))\mathbf{d}(t) \\
\mathbf{y}(t) &= \mathbf{C}(\mathbf{p}(t))\mathbf{x}(t) + \mathbf{D}(\mathbf{p}(t))\mathbf{u}(t) + \mathbf{D}_2(\mathbf{p}(t))\mathbf{d}(t) \\
\begin{pmatrix}\dot{\mathbf{x}}(t)\\ \mathbf{y}(t)\end{pmatrix} &= \mathbf{S}(\mathbf{p}(t))\begin{pmatrix}\mathbf{x}(t)\\ \mathbf{u}(t)\\ \mathbf{d}(t)\end{pmatrix} \\
\mathbf{S}(\mathbf{p}(t)) &= \begin{bmatrix}\mathbf{A}(\mathbf{p}(t)) & \mathbf{B}(\mathbf{p}(t)) & \mathbf{E}(\mathbf{p}(t))\\ \mathbf{C}(\mathbf{p}(t)) & \mathbf{D}(\mathbf{p}(t)) & \mathbf{D}_2(\mathbf{p}(t))\end{bmatrix},
\end{aligned} \tag{8}$$

where $\mathbf{p}(t) = [p_1(t) \dots p_R(t)]$ is the so-called parameter vector which consists of scheduling parameters $p_i(t)$, or simply the parameters. The $\mathbf{p}(t) \in \Omega^R \in \mathbb{R}^R$ is an R dimensional real vector within the $\Omega = [p_{1,min}, p_{1,max}] \times [p_{2,min}, p_{2,max}] \times \dots \times [p_{N,min}, p_{N,max}] \in \mathbb{R}^R$, $\forall p\ p_{i,min} < p_{i,max}$ hypercube inside the $\mathbb{R}^R$ real vector space.

B. CONTROL ORIENTED MODEL TRANSFORMATION

Control oriented model form is a widely used technique in control engineering if we apply different state feedback based control solutions [56]. In this way it is able to describe the deviation of the state variables from given predefined reference values which can be the model equilibrium (natural equilibrium) or prescribed values (enforced equilibrium). Thus, the so-called error dynamics is attached to the state variables. The usual state feedback based control solutions guarantee that the state variables become zero over time. Through this approach, the goal is to reach the zero state variables over time, which means that the state variables become equal to the predefined values or equilibrium – and the design of reference compensator is not necessary anymore [33], [34]. This tool is a convenient method for TP transformation based modeling and control as well.

Consider the $\mathbf{x}(t) \in \mathbb{R}^n$ state vector and the $\mathbf{x}_d \in \mathbb{R}^n$ (permanent) model equilibrium. The formalization is:

$$\Delta\mathbf{x}(t) = \mathbf{x}(t) - \mathbf{x}_d, \tag{9}$$

where $\Delta\mathbf{x}(t) \in \mathbb{R}^n$ is the deviation from the equilibrium and the goal of the control in this way is $\Delta\mathbf{x}(t) \to \mathbf{0}$.

Respect to (9), the (8) can be described in control oriented form as follows:

$$\begin{aligned}
\dot{\mathbf{x}}(t) - \mathbf{0} &= \Delta\dot{\mathbf{x}}(t) \\
&= \mathbf{A}(\mathbf{p}(t))\Delta\mathbf{x}(t) + \mathbf{B}(\mathbf{p}(t))\Delta\mathbf{u}(t) + \mathbf{E}(\mathbf{p}(t))\Delta\mathbf{d}(t) \\
\mathbf{y}(t) - \mathbf{y}_d &= \Delta\mathbf{y}(t) \\
&= \mathbf{C}(\mathbf{p}(t))\Delta\mathbf{x}(t) + \mathbf{D}(\mathbf{p}(t))\Delta\mathbf{u}(t) + \mathbf{D}_2(\mathbf{p}(t))\Delta\mathbf{d}(t) \\
\begin{pmatrix}\Delta\dot{\mathbf{x}}(t)\\ \Delta\mathbf{y}(t)\end{pmatrix} &= \mathbf{S}(\mathbf{p}(t)) \begin{pmatrix}\Delta\mathbf{x}(t)\\ \Delta\mathbf{u}(t)\\ \Delta\mathbf{d}(t)\end{pmatrix} \\
\mathbf{S}(\mathbf{p}(t)) &= \begin{bmatrix}\mathbf{A}(\mathbf{p}(t)) & \mathbf{B}(\mathbf{p}(t)) & \mathbf{E}(\mathbf{p}(t)) \\ \mathbf{C}(\mathbf{p}(t)) & \mathbf{D}(\mathbf{p}(t)) & \mathbf{D}_2(\mathbf{p}(t))\end{bmatrix},
\end{aligned} \tag{10}$$

where $\Delta\mathbf{x}(t) = \mathbf{x}(t) - \mathbf{x}_d$, $\Delta\mathbf{y}(t) = \mathbf{y}(t) - \mathbf{y}_d$, $\Delta\mathbf{u}(t) = \mathbf{u}(t) - \mathbf{u}_d$ and $\Delta\mathbf{d}(t) = \mathbf{d}(t) - \mathbf{d}_d$ are the deviation based state-, output-, control input- and disturbance input-vectors, respectively. For our case the following equilibrium has been applied: $\mathbf{x}_d = [D_{1,d}, D_{2,d}, S_{1,d}, S_{2,d}, G_d, X_d, I_d]^\top = [0, 0, 0, 0, G_B, 0, I_B]^\top$, $u_d = 0$ and $d_d = 0$.

The model described by (1a) - (1g) can be written as it is represented by (10). Regarding the measurable state $G(t)$ from (1e), its form becomes:

$$\begin{aligned}
\dot{G}(t) - 0 &= -(p_1 + X(t))G(t) + p_1\, G_B + \frac{1}{\tau_D} D_2(t) \\
&\quad - \Big[-(p_1 + X_d)G_d + p_1\, G_B + \frac{1}{\tau_D} D_{2,d} \Big] \\
&= -(p_1 + X_d)\Delta G(t) - G(t)\Delta X(t) + \frac{1}{\tau_D}\Delta D_2(t)
\end{aligned}$$

$$\mathbf{S}(\mathbf{p}(t)) = \begin{bmatrix}\mathbf{A}(\mathbf{p}(t)) & \mathbf{B} & \mathbf{E} \\ \mathbf{C} & \mathbf{D} & \mathbf{D}_2\end{bmatrix} \tag{11}$$

$$= \begin{bmatrix}
-\frac{1}{\tau_D} & 0 & 0 & 0 & 0 \\
\frac{1}{\tau_D} & -\frac{1}{\tau_D} & 0 & 0 & 0 \\
0 & 0 & -\frac{1}{\tau_S} & 0 & 0 \\
0 & 0 & \frac{1}{\tau_S} & -\frac{1}{\tau_S} & 0 \\
0 & \frac{1}{\tau_D} & 0 & 0 & -(p_1 + X_d) \\
0 & 0 & 0 & 0 & 0 \\
0 & 0 & 0 & \frac{1}{\tau_S} & 0 \\
0 & 0 & 0 & 0 & 1 \\
0 & 0 & 0 & \frac{1000A_g}{M_{wG}V_G}C \\
0 & 0 & 0 & 0 \\
0 & 0 & \frac{1}{V_I} & 0 \\
0 & 0 & 0 & 0 \\
-G(t) & 0 & 0 & 0 \\
-p_2 & p_3 & 0 & 0 \\
0 & -n & 0 & 0 \\
0 & 0 & 0 & 0
\end{bmatrix} \tag{12}$$

By applying the same transformation on the remaining state equations, the deviation-based control oriented state-space description can be represented by its system matrix $\mathbf{S}(\mathbf{p}(t))$ in (11). The only nonlinearity causing term is the multiplication with $G(t)$ in (11) – thus, we have selected the measurable state $G(t)$ as scheduling variable, namely $\mathbf{p}(t) = p(t) = G(t)$. We have already presented in Sec. II-C that the aim of the control is to keep $G(t)$ within 60 [mg/dL] and 320 [mg/dL] – which is considered as the physiologically optimal range [6], [10]. This leads to the $\Omega^1 = [G_{min}, G_{max}] = [60, \dots, 320]$ one dimensional parameter space where the $p(t)$ can be changed. Furthermore, only $\mathbf{A}(\mathbf{p}(t))$ is affected by $p(t)$.

C. TP BASED MODEL TRANSFORMATION

The TP model transformation is able to transform a given function into its TP function form within given limitations [57]. The transformation is possible in case of multi-variable functions, neural networks, fuzzy constructs, among others. Due to its flexibility, it is possible to use the TP model transformation to transform a given model described by its LPV (or qLPV) representation into polytopic TP model form as well [34]. In more detail, the TP model transformation is capable of transforming a given model into multiplications consisting of orthonormal weighting function systems both depending on one variable, namely, the $p(t)$ scheduling variable. The resulting TP model is able to approximate the

original LPV model with given accuracy depending on the applied specifications. The sampling density is connected to the higher order singular value decomposition (HOSVD) among others. The TP model transformation can be combined with LMI-based controller design – the developed sub-controllers can be connected by the occurring weighting functions and the resulting controller becomes equal to the convex combination of them [34], [58].

In order to realize the TP model transformation the (8) can be considered where the bounded Ω hypercube – interpreted inside the $\mathbb{R}^R$ vector space – is the transformational space. In the following, we introduce the main terms and structures which are needed to execute the TP model transformation on a given class of LPV models.

Definition 1: The finite element convex polytopic model describes the $\mathbf{S}(\mathbf{p}(t))$ actual model as a convex combination of the $\mathbf{S}_r \in \mathbb{R}^{(n+k)\times(n+m+l)}$ LTI sub-models – LTI vertices – inside the Ω hypercube in the following way:

$$\mathbf{S}(\mathbf{p}(t)) = \sum_{r=1}^{R} w_r(\mathbf{p}(t))\mathbf{S}_r, \tag{13}$$

where the R is limited as described above and $w_r(\mathbf{p}(t)) \in [0, 1]$ is a continuous convex weighting function.

Definition 2: The finite element TP type convex polytopic model describes the $\mathbf{S}(\mathbf{p}(t))$ actual model as a convex combination of the $\mathbf{S}_r \in \mathbb{R}^{(n+k)\times(n+m+l)}$ LTI vertex system inside the Ω hypercube in the following way:

$$\begin{aligned}\mathbf{S}(\mathbf{p}(t)) &= \sum_{i_1=1}^{I_1}\sum_{i_2=1}^{I_2}\cdots\sum_{i_R=1}^{I_R}\prod_{r=1}^{R} w_{r,i_r}(p_r(t))\mathbf{S}_{i_1,i_2,\ldots,i_R} \\ &= \mathcal{S}\overset{\mathrm{R}}{\underset{\mathrm{r=1}}{\boxtimes}}\mathbf{w}_r(p_r(t)),\end{aligned} \tag{14}$$

where $\mathcal{S} \in \mathbb{R}^{I_1\times I_2\times\ldots\times I_R\times(n+k)\times(n+m+l)}$ coefficient tensor can be derived from the $\mathbf{S}_{i_1,i_2,\ldots,i_R}$ LTI vertex system and the $\mathbf{w}_r(p_r(t))$ weighting function vector consists of the $w_{r,i_r}(p_r(t))$ $(i_r = 1\ldots I_R)$ univariate continuous weighting functions.

Definition 3: The HOSVD method [34], [35], [59] makes it possible to construct a tensor product structure according to the significance of each component. The result of the TP model transformation is the numerical reconstruction of the HOSVD of the given LPV model without the consideration of complexity reduction and convex hull manipulation. The resulting HOSVD canonical form consists of singular functions in orthonormal structure and a core tensor consists of LTI system vertices assigned to the higher order singular values.

Definition 4: A general convex hull can be defined in the following way:

$$\mathrm{Conv}(\Omega) = \left\{\sum_{i=1}^{|\Omega|} w_i q_i | (\forall i : w_i \geq 0) \wedge \sum_{i=1}^{|\Omega|} w_i = 1\right\}, \tag{15}$$

where Ω is the convex set, w_i are the weighting parameters and q_i are the points inside Ω. Namely, the Ω can be defined with a convex combination of w_i and q_i, if $q_i \in \Omega$ [60].

Definition 5: Convex resulting TP model occurs, if the weighting functions satisfy the following criteria:

$$\begin{aligned}&\forall r, i, p_r(t) : w_{r,i_r}(p_r(t)) \in [0, 1] \\ &\forall r, p_r(t) : \sum_{i=1}^{I_R} w_{r,i_r}(p_r(t)) = 1.\end{aligned} \tag{16}$$

Definition 6: The minimum volume simplex (MVS) kind of convex hull is the smallest convex region to be defined inside the parameter space [35]. In this case $(\mathcal{S})_{j_r=j}$ r-mode sub-tensors evolve a minimal volume bounding simplex for $\mathcal{S} \times_r \mathbf{w}_{jr}^{(r)}(p_r)$ trajectory over $r = 1..R$ for the $\mathcal{S} \in \mathbb{S}^{I_1\times\ldots\times I_R}$ core tensor, which is realized from the $\mathbf{S}_{i_1,\ldots,i_R}$ matrices as follows:

$$\mathbf{S}(\mathbf{p}) = \mathcal{S}\overset{\mathrm{R}}{\underset{\mathrm{r=1}}{\boxtimes}}\mathbf{w}^{(r)}(p_r). \tag{17}$$

Definition 7: The control input in case of a general state-feedback controller can be described as

$$\mathbf{u}(t) = \mathbf{K}(\mathbf{p}(t))\mathbf{x}(t), \tag{18}$$

where $\mathbf{K}(\mathbf{p}(t)) \in \mathbb{R}^{m\times n}$ is the parameter dependent controller gain. A kind of state-feedback controller, the parallel distributed controller in polytopic structure can be described in the following way:

$$\mathbf{K}(\mathbf{p}(t)) = \mathcal{K}\overset{\mathrm{R}}{\underset{\mathrm{r=1}}{\boxtimes}} w_r(p_r(t)) = \mathcal{K} \times_r w(\mathbf{p}(t)). \tag{19}$$

Further derivations, explanations and case studies can be found in [34]–[45], [58], [61], [62].

We have used the TP Toolbox [63] in this study in order to execute the TP model transformation and get the appropriate weighting functions belonging to the given TP model form.

D. THE REALIZED TP MODEL FORM

By applying the TP model transformation on (11), the general TP model structure becomes $\mathbf{S}(G(t)) = \mathcal{S} \times_1 \mathbf{w}(G(t))$.

The variation of the obtained MVS type weighting functions can be seen on Fig. 1. The obtained resulting weighting functions are linear due to the properties of the model described by (11).

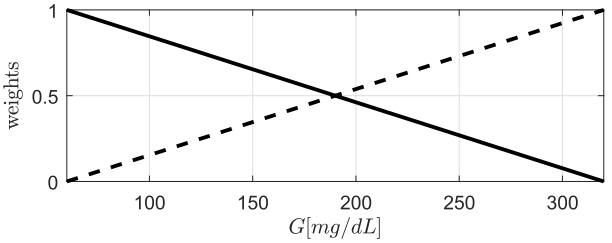

FIGURE 1. The w($G(t)$) weighting function regarding the realized TP model transformation.

The resulting specific TP model form in this case becomes

$$S(G(t)) = \mathcal{S} \times_1 w_1(G(t)), \tag{20}$$

namely, $\mathcal{S} = [\mathbf{S}(G_{min}), \mathbf{S}(G_{max})]$.

IV. LMI BASED CONTROLLER DESIGN

Several LMI based methods are available for controller design to get the $\mathcal{K}$ feedback gain tensor [64], [65]. Due to the disturbance input – glucose intake – we have selected the robust pole clustering method for the controller design via LMI optimization [66], [67]. By applying this method the poles of the closed-loop system lie inside the so-called LMI-region on the complex plane.

Definition 8 [54]: "A given subset $\mathcal{D}$ inside the complex plane is an LMI region if there exists a $\alpha = [\alpha_{kl}] \in \mathbb{R}^{m\times m}$ symmetric matrix and a $\beta = [\beta_{kl}] \in \mathbb{R}^{m\times m}$ matrix such that

$$\mathcal{D} = \{s \in \mathbb{C} : \ f_{\mathcal{D}}(s)\} < 0$$
$$f_{\mathcal{D}}(s) := \alpha + s\beta + \bar{s}\beta^{\top} = [\alpha_{kl} + \beta_{kl}s + \beta_{lk}\bar{s}]_{1\le k,l\le m}, \quad (21)$$

where $f_{\mathcal{D}}(s)$ characteristic function takes values in the space of $m \times m$ Hermitian matrices and < 0 means negative definite."

Theorem 1: The matrix $\mathbf{A}$ *is* $\mathcal{D}$ *stable if and only if there exists a positive definite symmetric matrix* $\mathbf{X}$ *such that*

$$\begin{aligned} \mathbf{X} &> 0 \\ M_{\mathcal{D}}(\mathbf{A},\mathbf{X}) &< 0 \\ M_{\mathcal{D}}(\mathbf{A},\mathbf{X}) &= \alpha \otimes \mathbf{X} + \beta \otimes (\mathbf{AX}) + \beta^{\top} \otimes (\mathbf{AX})^{\top} \\ &= [\alpha_{ab}\mathbf{X} + \beta_{ab}(\mathbf{AX}) + \beta_{ba}(\mathbf{AX})^{\top}]_{ab}, \end{aligned} \quad (22)$$

where $M_{\mathcal{D}}$ *is a* $m \times m$ *block matrix characterizes the pole location in a given LMI region.*

Proof can be found in [54], [66], [68].

In the following, we introduce the design method and the stability on intersection of LMI regions.

If i pieces of given $\mathcal{D}_i$ LMI regions are specified then the $\mathbf{A}$ matrix is $\mathcal{D}$ stable if and only if there exists a positive definite, symmetric matrix $\mathbf{X}$ such that

$$\begin{aligned} \mathbf{X} &> 0 \\ M_{\mathcal{D}}(\mathbf{A},\mathbf{X})_i &< 0, \quad \forall i \in \mathbb{N}. \end{aligned} \quad (23)$$

The following substitution can be applied to $f_{\mathcal{D}}(s)$ (21) and $M_{\mathcal{D}}(\mathbf{A},\mathbf{X})$ (22):

$$(\mathbf{X}, (\mathbf{AX}), (\mathbf{AX})^{\top}) \leftrightarrow (1, s, \bar{s}). \quad (24)$$

Note that in case of the closed loop, the following substitutions can be applied by introducing the $\mathbf{L} \in \mathbb{R}^{m\times n}$ term as follows:

$$(\mathbf{X}, (\mathbf{AX}+\mathbf{BL}), (\mathbf{AX}+\mathbf{BL})^{\top}) \leftrightarrow (1, s, \bar{s}), \quad (25)$$

from where the $\mathbf{K}$ controller gain can be calculated as

$$\mathbf{K} := \mathbf{LX}^{-1}. \quad (26)$$

By considering the general $\mathcal{D}$ stability determined by (22) – (25) then, along the lines of [69], [70], the so-called α-stability and disk kind of LMI regions can be defined in presence of disturbance as follows:

$$2\alpha\mathbf{X} + (\mathbf{AX}+\mathbf{BL}) + (\mathbf{AX}+\mathbf{BL})^{\top} + \mathbf{EE}^{\top} < 0, \quad (27a)$$
$$\begin{bmatrix} -r\mathbf{X} & q\mathbf{X} + (\mathbf{AX}+\mathbf{BL}) \\ q\mathbf{X} + (\mathbf{AX}+\mathbf{BL})^{\top} & -r\mathbf{X} \end{bmatrix} < 0, \quad (27b)$$

where the $\mathbf{K} = \mathbf{LX}^{-1}$ in agreement with (26).

The α-stability kind of region described by (27a) determines a half-plane on the negative left hand side and ensures that all of the closed loop poles lie on this plane. In this case, the α tuning parameter can be interpreted as the distance between the imaginary axis and the half-plane.

The disk kind of region described by (27b) determines a disk plane in the complex domain and ensures that all of the poles of the closed system lie inside this plane. The tuning parameters are the q and r variables, which can be interpreted as the center and the radius of the disk plane, respectively.

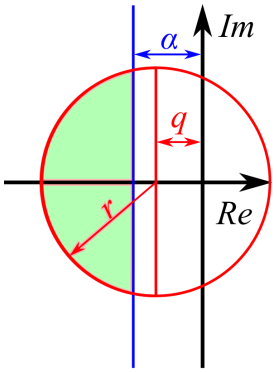

FIGURE 2. The $\mathcal{D}$ regions method allows that the poles of the closed loop system will lie within the shaded region thank to the applied α-stability and disk kind of LMI regions.

Figure 2. provides a graphical interpretation of the detailed techniques. The resulting feedback gain provide that the poles of the closed-loop system lie in the shaded region.

In case of LPV systems, the use of the introduced LMI techniques from (27a) – (27b) are still possible. In accordance with [66], [69], [70] the following feasibility kind of LMI optimization problem needed to be solved in order to get the $\mathbf{K}_i$ subcontrollers belong to the $\mathbf{S}_i$ LTI vertices of the system which ensures the stability and prompt control action for the (11). Note that $\mathbf{K}_i$ and $\mathbf{S}_i$ denote $\mathbf{K}(p_i)$ and $\mathbf{S}(p_i)$ where $p_i = [G_{min}, G_{max}]$. However – for sake of simplicity – we applied a short notation in the followings.

$$\mathbf{X} > 0, \quad (28a)$$
$$2\alpha\mathbf{X} + (\mathbf{A}_i\mathbf{X} + \mathbf{BL}_i) + (\mathbf{A}_i\mathbf{X} + \mathbf{BL}_i)^{\top} + \mathbf{EE}^{\top} < 0, \quad (28b)$$
$$\begin{bmatrix} -r\mathbf{X} & q\mathbf{X} + (\mathbf{A}_i\mathbf{X} + \mathbf{BL}_i) \\ q\mathbf{X} + (\mathbf{A}_i\mathbf{X} + \mathbf{BL}_i)^{\top} & -r\mathbf{X} \end{bmatrix} < 0,$$
$$i < j \ \text{ s.t. } \ w_i \cap w_j \neq \phi. \quad (28c)$$

In order to get the $\mathbf{K}(p_i)$ controller gains, we have to solve the optimization problem described by (28a) – (28c). This provides stable controller gains in Lyapunov sense which satisfy the predefined criteria against the poles of the closed loop. It should be noted that we have applied MOSEK Apps. solver [71] and the YALMIP toolbox [72] to solve the LMI optimization problem described by (28a) – (28c).

Remark 1: The proposed difference based LPV system in (11) *is not fully controllable, because* $\text{rank}(\mathcal{C}(\mathbf{A},\mathbf{B})) = 5$, $n = 7$, *where* $\mathcal{C}$ *is the controllability matrix. Hence, two*

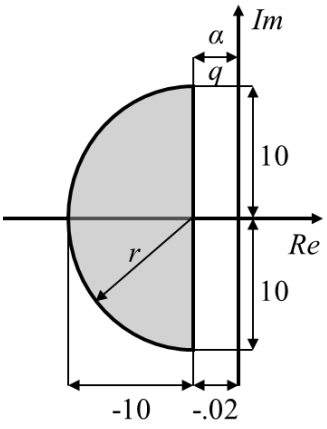

FIGURE 3. The resulting controller ensures that the poles lie in the shaded region in accordance with the applied values of α, r and q.

uncontrollable modes appear in the system. Both uncontrollable modes are stable, namely, both of them decay to zero asymptotically (the eigenvalues do have negative real parts) and all of the unstable modes are controllable. Therefore, the system is stabilizable [73].

The two uncontrollable, but stable modes are $\lambda_{uc,1-2} = -0.025$ which requires the selection of α and q to cover them in order to satisfy (28a) – (28b). In accordance with this requirement, we have selected $\alpha = 0.02$ and $q = -0.02$ which are basically equivalent statements and this selection guarantees that all of the closed loop poles lay beyond -0.02 at the negative half plane. In order to reach satisfactory gains on the oscillation and magnitude points of view, we have selected that $r = 10$ which cause that all of real parts of the poles obtained will be between -10.02 and -0.02.

Based on (26) the controller gains can be calculated as $\mathbf{K}_i = \mathbf{L}_i\mathbf{X}^{-1}$.

After the optimization, the following $\mathbf{K}_i$ gains have been obtained:

$$\begin{aligned}\mathbf{K}_1 &= \mathbf{K}(G_{min}) \\ &= \big[-1.0414 \quad 11.4231 \quad -28.5733 \quad -58.1709 \\ &\quad 10.5541 \quad -1.537 \cdot 10^5 \quad -90.5105\big] \end{aligned} \tag{29}$$

and

$$\begin{aligned}\mathbf{K}_2 &= \mathbf{K}(G_{max}) \\ &= \big[-1.0308 \quad 11.396 \quad -28.5111 \quad -58.0372 \\ &\quad 10.5171 \quad -1.5346 \cdot 10^5 \quad -90.2944\big] \end{aligned} \tag{30}$$

which leads to $\mathcal{K} = [\mathbf{K}(G_{min}), \mathbf{K}(G_{max})]^\top$.

The large $\mathbf{K}(1,6)_i$ elements are caused by the small p_3 model parameter – the magnitude of which is 10^{-5}. As the gains are close to each other, soft control action can be expected.

Figure 4. shows the calculated poles of the closed loop system at the extremes of the parameter domain $(\lambda(\mathbf{A}_i + \mathbf{BK}_i)_i)$ – in the simulation environment. As it can be seen, the poles lie in the determined LMI region, which is parametrized by the α, q and r parameters.

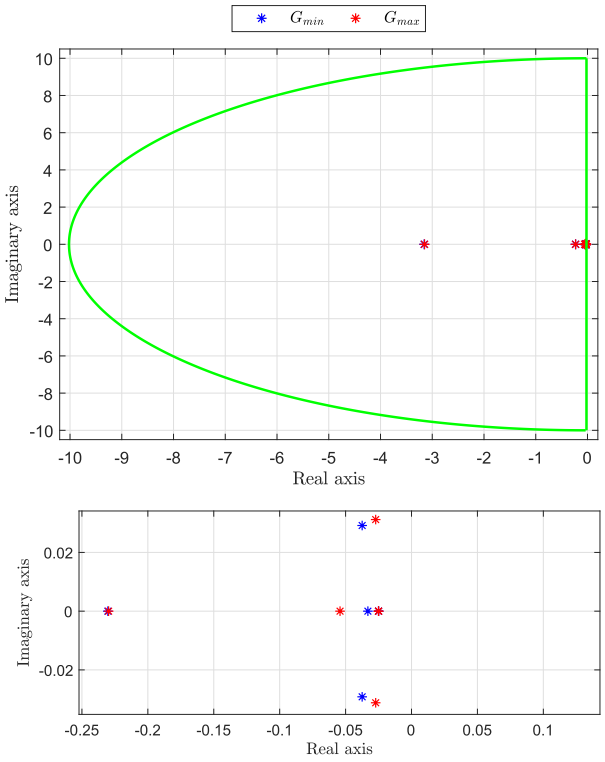

FIGURE 4. Closed loop poles $(\lambda(\mathbf{A}_i + \mathbf{BK}_i)_i)$ belong to the vertices of the LPV systems. The upper diagram is an overview about the whole complex plane with the selected LMI region. It can be seen that all of the closed loop poles lie inside the determined LMI region. The lower figure points out the complex plane from 0 to -0.26 from the real values point of view. It can be seen that the poles lie in the LMI region, namely, $\text{Re}(\lambda)_i < -0.02$ in accordance with the selected α and q. The lower diagram shows the poles of the system which are closed to zero from the upper diagram.

V. DESIGN OF MIXED ADDITIVE/NON-ADDITIVE EXTENDED KALMAN FILTER

As only the blood glucose level $G(t)$ can be directly measured we need to estimate the remaining states as well. We designed a specific Extended Kalman Filter (EKF) in order to estimate the values of the states. Since the carbohydrate intake in our glucose metabolism model and the measurement noise is also an additive term, the overall system can be given in the following form:

$$\begin{aligned}\dot{\mathbf{x}} &= f(\mathbf{x}(t), \mathbf{u}(t)) + \mathbf{d}(t) \\ \mathbf{z}_k &= \mathbf{C}\mathbf{x}_k + \mathbf{v}_k, \end{aligned} \tag{31}$$

where $\mathbf{x}(t)$ is the actual state, $\mathbf{u}(t)$ is the actual control signal, $\mathbf{w}(t)$ is the actual disturbance. $\mathbf{v}_k$ is the actual sensor noise, $\mathbf{C}$ is the output matrix. $\mathbf{z}$ output of the system is linearly dependent on the BG level and on the sensor noise.

The $\mathbf{d}(t)$ impulse, as a disturbance, affects the corresponding states. The values of the $n \times n$ semidefinite $\mathbf{Q}(t)$ covariance matrix had to be selected with the consideration of the effect of the disturbance on each state.

In this given case we modeled the sensor noise with a CGMS model described in II-B, however – the $\mathbf{v}_k$ – term was approximated with zero mean and 10 [mg/dL] variance $\mathbf{v}_k \sim \mathcal{N}(0, \mathbf{R}_k)$ with $\mathbf{R}_k$ covariance matrix. The variance has been arbitrarily selected in this specific case, but in accordance with the latest findings of [74].

In the light of the aforementioned considerations, the prediction and update algorithm of the EKF can be described as follows.

Predict phase

Predicted state estimate:

$$\dot{\hat{\mathbf{x}}}(t) = f(\hat{\mathbf{x}}(t), \mathbf{u}(t)). \tag{32}$$

Predicated covariance estimate:

$$\dot{\mathbf{P}}(t) = \mathbf{F}(t)\mathbf{P}(t) + \mathbf{P}(t)\mathbf{F}(t)^\top + \mathbf{Q}(t), \tag{33}$$

where $\mathbf{F}(t) = \frac{\partial f}{\partial \mathbf{x}}\Big|_{\hat{\mathbf{x}}(t),\mathbf{u}(t)}$, $\hat{\mathbf{x}}_{k+1,k} = \hat{\mathbf{x}}(t_k)$ and $\mathbf{P}_{k+1,k} = \mathbf{P}(t_k)$ by applying appropriate sampling.

Update phase

Innovation residual:

$$\tilde{\mathbf{y}}_{k+1} = \mathbf{z}_{k+1} - \mathbf{C}\hat{\mathbf{x}}_{k+1|k}. \tag{34}$$

Innovation covariance:

$$\mathbf{S}_{k+1} = \mathbf{C}\mathbf{P}_{k+1|k}\mathbf{C}^\top + \mathbf{R}_{k+1}. \tag{35}$$

Kalman gain:

$$\mathbf{K}_{k+1} = \mathbf{P}_{k+1|k}\mathbf{C}^\top\mathbf{S}_{k+1}^{-1}. \tag{36}$$

Updated state estimate:

$$\hat{\mathbf{x}}_{k+1|k+1} = \hat{\mathbf{x}}_{k+1|k} + \mathbf{K}_{k+1}\tilde{\mathbf{y}}_{k+1}. \tag{37}$$

Updated covariance estimate:

$$\mathbf{P}_{k+1|k+1} = (\mathbf{I} - \mathbf{K}_{k+1}\mathbf{C})\mathbf{P}_{k+1|k}, \tag{38}$$

where $\mathbf{I}$ is the unit matrix and $\mathbf{C}$ is the output matrix, respectively [75], [76].

Due to the model specificities, the applied sampling time for the EKF was 1 min because our primary goal was the demonstration of the usability of the TP-LMI-LPV controller. Further development regarding sensor modeling will be done in our future work.

VI. FINAL CONTROL STRUCTURE

Figure 5. presents the developed control structure. The *Original Nonlinear Model* is described by (1a) - (1g). The output of the model is the $y(t) = G(t)$ blood glucose level which is affected by the $v(t)$ additive random sensor noise. The measured output is the $z(t) = y(t) + v(t)$. The *Extended Kalman Filter* provides the $\hat{\mathbf{x}}_{EKF}(t)$ estimated states from which the deviation based estimated states are generated as $\Delta\hat{\mathbf{x}}_{EKF}(t) = \hat{\mathbf{x}}_{EKF}(t) - \mathbf{x}_d$. The deviation based error $\Delta e(t)$ is based on a comparison between the reference and estimated states, namely, $\Delta\mathbf{e}(t) = \Delta\mathbf{r} - \Delta\hat{\mathbf{x}}_{EKF}(t)$. The applied $\Delta\mathbf{r} = \mathbf{0}_{7\times1}$ reference was constant zero, which basically means the zero deviation of $\mathbf{x}(t)$ through $\hat{\mathbf{x}}_{EKF}(t)$ from the desired states $\mathbf{x}_d$.

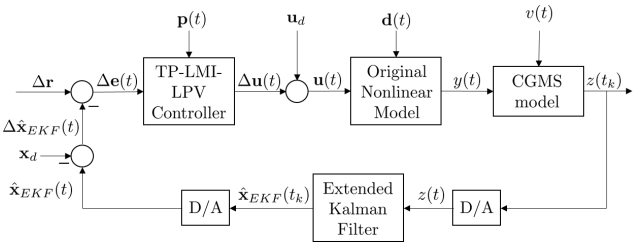

FIGURE 5. Final control structure with the designed TP-LMI-LPV controller and mixed EKF. The D/A converter is added to provide the continuous signal to the continuous process model used by the EKF in the predict phase.

The controller directly gets information about the scheduling parameter $\mathbf{p}(t) = p(t) = G(t)$, which was in this case the measured parameter and provides the appropriate difference based control signal $\Delta\mathbf{u}(t)$. The applied control signal can be calculated as $\mathbf{u}(t) = \Delta\mathbf{u}(t) + \mathbf{u}_d$.

It should be noted that we applied the filtered BG level instead of the measured one ($p(t) = G_{EKF}(t) \neq z(t)$), since it is accessible and in this way we were able to reduce the high noise on it.

VII. NUMERICAL SIMULATIONS

A. INITIAL CONDITIONS AND CIRCUMSTANCES

The developments have been made under the MATLAB core – although, we did use the already mentioned external solvers – YALMIP [72] framework and MOSEK [71] solver – to solve the optimization problems. We have applied Runger-Kutta 4 method [77] for the simulations.

We have started the simulations by using the following initial state variables: $\mathbf{x}(t_0) = [0, 0, 0, 0, 110, 0, 5]^\top$. We expected that no food and insulin intakes have been done before t_0, thus the corresponding state variables have been taken to be zero: $\mathbf{x}_{1-4}(t_0) = 0$. The initial state values belonging to $G(t_0)$, $X(t_0)$ and $I(t_0)$ have been arbitrarily, but realistically selected. The $\mathbf{x}_{cv}(t_0) = [0, 0, 0, 0, 110, 0, 5]^\top$ – the initial states of the cross-validation system have been considered as the same as $\mathbf{x}(t_0)$ in order to facilitate the comparability. The $\hat{\mathbf{x}}_{EKF}(t_0) = [0, 0, 0, 0, 130, 0, 11]^\top$. We assumed the same for $\hat{\mathbf{x}}_{EKF,1-4}(t_0)$ as in case of $\mathbf{x}_{1-4}(t_0)$, namely, nor food neither insulin have been taken before the beginning of the simulation. The $\hat{\mathbf{x}}_{EKF,5-7}(t_0)$ have been arbitrarily selected, but comparable to $\mathbf{x}_{5-7}(t_0)$ to simulate the uncertainty of the EKF at the beginning of the simulation.

We did use $\Delta\mathbf{r} = \mathbf{0}_{7\times1}$ as permanent reference signal.

During our investigations we have applied multiple randomized disturbance signal – both the time instances and the amounts of food intake were randomized within a given range. The glucose absorption submodel using the CHO intake and the given utilization rate (A_g). During the CHO intake design we applied the dietary recommendations for diabetic patients [78]–[81]. We decided to use 300 $\pm$ 50 g on a daily basis (which is higher than the recommended 300 g CHO/day) and split it into 5 meals in order to simulate high glucose load. In order to approach "eating" realistically,

TABLE 2. Applied meal intakes on daily basis.

	Time instance [min]	Amount of intake [g]
First meal	$30 + 5 \cdot randn$	$90 + 10 \cdot randn$
Second meal	$220 + 5 \cdot randn$	$15 + 10 \cdot randn$
Third meal	$400 + 5 \cdot randn$	$100 + 10 \cdot randn$
Fourth meal	$720 + 5 \cdot randn$	$15 + 10 \cdot randn$
Fifth meal	$980 + 5 \cdot randn$	$80 + 10 \cdot randn$

we assumed the consumption of 20 g of CHO at given time instances. For example, if the total amount of CHO was 108 g in a meal then the developed algorithm realized five portion of 20 g of CHO and one portion of 8 g of CHO at consecutive time instances. Furthermore, we added a saturation to all intakes to avoid negative intakes which may appear due to the applied randomization method. In this way we were able to test our control solution under ''unfavorable'' conditions to investigate its abilities. We have applied standard normal distribution ($randn = \mathcal{N}(0, 1)$) for the randomization. The exact details regard to the meal protocol can be found in Table 2.

We have simulated the operation of the system on daily basis, namely, we simulated 1440 minutes (24 hours) in each secondary loop. Further, we did long-term tests with a total duration of 30 days. Hence, 30 iterations have been done in the primary loop.

B. RESULTS

Figure 6–10. represent one day, namely, 1440 minutes – the first day of the 30 days long test. Through these diagrams we introduce the operation of the control framework in details. It should be noted that in those diagrams representing the BG levels we show the results in [mmol/L] – which is usually applied in the medical community; in other diagrams some values are represented in [mg/dL]. The model uses [mg/dL], thus we considered this unit during the control design and calculations. We applied the exchange rate of 18.018 [mg/dl] = 1 [mmol/L].

Figure 6. shows the $d(t)$ disturbance and $u(t)$ control inputs, respectively. It can be seen that the controller became active right after the disturbance intake in order to decrease the error.

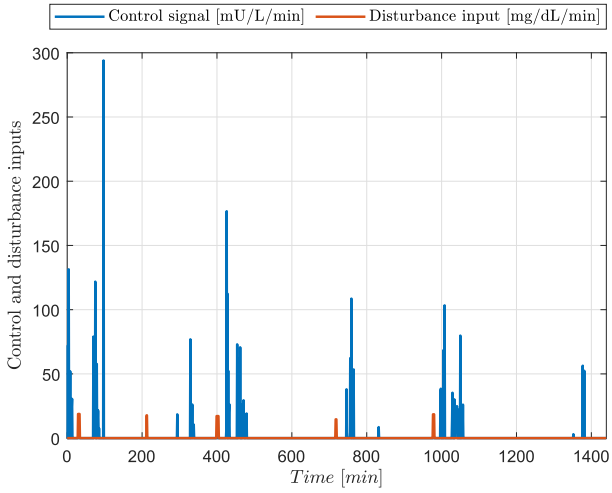

FIGURE 6. The applied control and disturbance signals. The upper figure shows the d(*t*) disturbance signal in accordance with the applied glucose intake protocol. The lower figure shows the u(*t*) control signal provided by the controller.

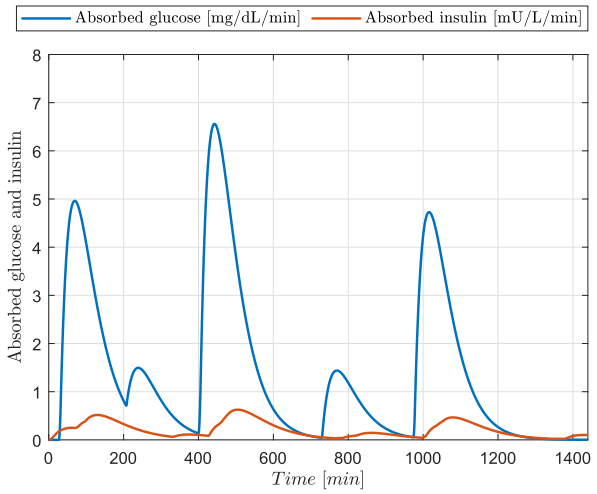

FIGURE 7. Appearance of the absorbed insulin ($S_2(t)$) and carbohydrate ($D_2(t)$) in the blood.

Figure 7. shows the absorbed glucose ($D_2(t)/\tau_D$) and insulin ($S_2(t)/\tau_S$) over time. Due to the model specificities (insulin distribution volume and time constants) the rate of absorption of insulin is delayed and ridden compared to the effect of glucose.

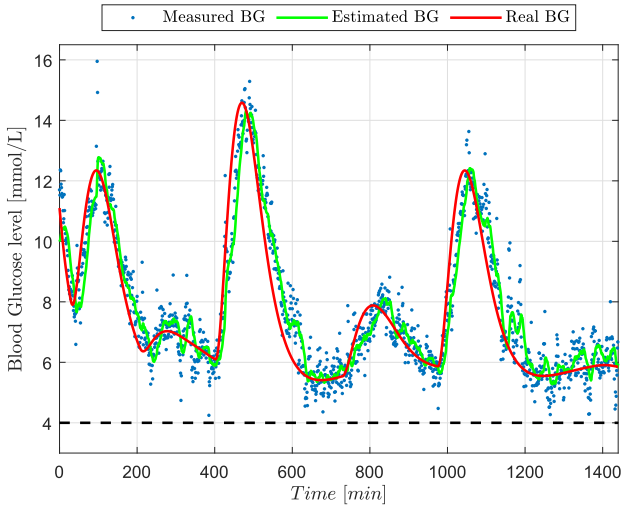

FIGURE 8. Measured, estimated and real blood glucose level during a 24 hours long simulation under the surveillance of the developed control scheme.

Figure 8. represents the blood glucose levels, namely the blood glucose concentration measured by the sensor, estimated by the EKF and the real blood glucose level. The specificities of $v(t)$ noise signal was already described previously.

Our goal was to use the EKF to demonstrate the usability of the proposed control solution. As the operation is possible without smoother, we did not implement EKF smoother in this case. The consequence is noisier EKF signals, however, this can be handled as an other source of uncertainty and based on the results, the proposed control solution is able to deal with it.

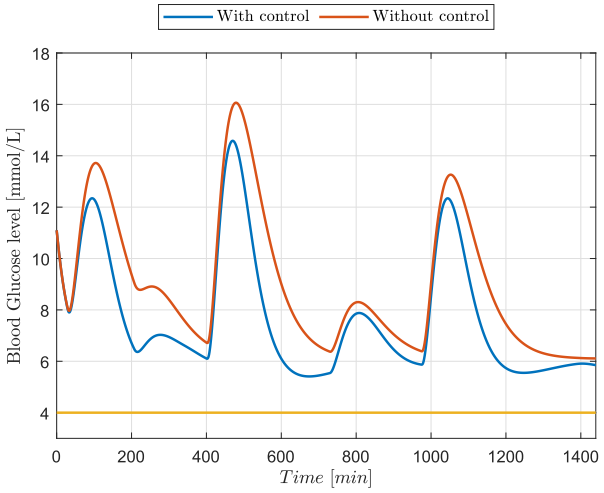

FIGURE 9. Numerical simulation of a 24 hours period. The controller was able to avoid the hypoglycemia despite the high glucose load.

Figure 9. shows the variation of the BG level with and without control. It is clearly visible that the controller provided better performance with lower peaks and the total time of hyperglycemia was also much lower by applying the developed controller.

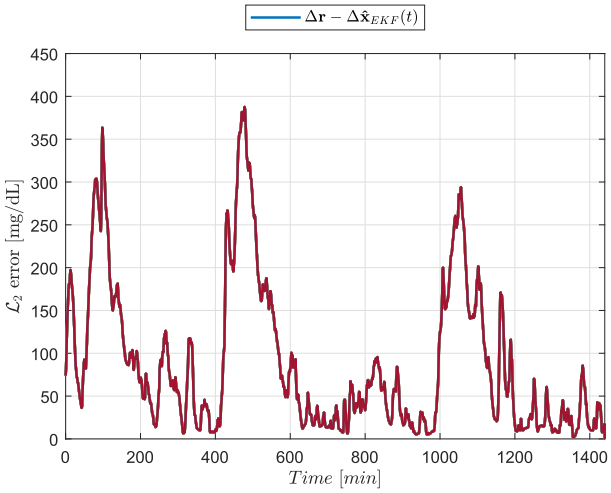

FIGURE 10. Comparison between the deviation based reference and deviation based estimated states within a 24 hours period.

Figure 10. represents the $\mathcal{L}_2$ norm [82] of the $\Delta\mathbf{e}(t)$ error signal. The selection of $\mathcal{L}_2$ norm was arbitrarily in order to make the graphical representation of the obtained error signal easier. This error representation is quite convenient – instead of comparing all the state variables $\mathbf{x}(t)_i$ by each other state-by-state the norm-based error provides all error information in one single vector which can be represented in a single diagram. As usual in state feedback controllers, the control goal was to reach the zero error over time $\Delta\mathbf{e}(t) \leftarrow \mathbf{0}$. Due to the control framework this is equivalent to the reaching of the zero deviation based states, since the deviation based reference signal was zero ($\Delta\mathbf{r} = \mathbf{0}$). In other words, when the state variables approach the zero value, the real state variables and the desired equilibrium are closing to each other. It can be seen on the figure that our controller solution is able to enforce the deviation based state variables to approach the zero over time. Hence, without disturbance the error signal the deviated state variables are closing to the zero. The fluctuation in the signal is coming from that simple fact that the states to be used for the comparison are provided by the EKF ($\Delta\mathbf{x}_{EKF}(t)$). From the fact that we did not use EKF smoother, the estimation error is reflected in the error signal as well.

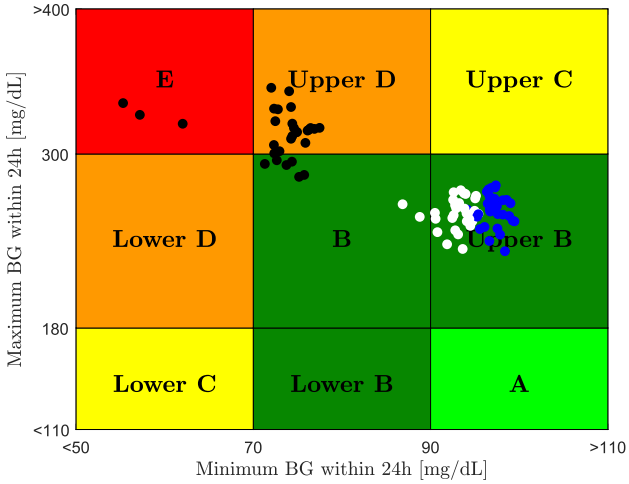

FIGURE 11. CVGA plot of the blood glucose levels within 24 hours during 30 days long simulation. Black dots: Measured BG level with sensor noise; White dots: Estimated BG by EKF; Blue dots: Real BG levels.

Figures 11. and 12. summarize the results of the long-term simulations (30 days) from quality and quantity point of view.

Figure 11. shows the control variability grid analysis (CVGA) diagram [83]. Basically, the diagram points out the lowest (horizontal axis) and the highest (vertical axis) BG levels on daily basis. Namely, each point belongs to the given minimum and maximum BG levels occurring on the same simulated day (within a 24 hours long period). The black dots belong to the measured values (the model output loaded by the simulated sensor noise), the white dots belong to the estimated values (produced by the EKF) and the blue dots belong to the real values (the model output without any noise), respectively.

Figure 12. is a scatter plot in which the controlled (green) and uncontrolled (red) cases are showed. Each dot represents the mean BG level of a given 24 hours long period in the same division as in case of Fig. 11. Thus, while the CVGA represents the extremes, the scatter plot represents the mean

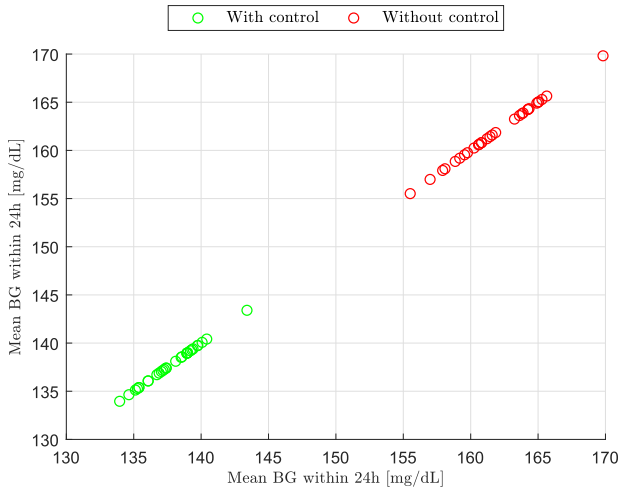

FIGURE 12. Scatter plot of the appeared mean blood glucose levels within 24 hours during 30 days long simulation by using the developed control structure and without it (only natural behavior of the model).

values of the same time period. It is clearly visible that the controller performed well, since it kept the mean BG level in a narrow $132 < G(t) < 145$ [mg/dL] range.

VIII. DISCUSSION

When we evaluate the results we have to analyze the specificities of the model first. Neither the control signal, nor the disturbance signal can be obtained immediately because of the time coefficients of the applied absorption submodels. Therefore, during the controller design only soft control actions – which can be translated as applying slower poles in the closed loop – should be used in the given framework to avoid over compensation, namely, overdosing the insulin. This can be improved by limiting the input and output signals by using appropriate LMIs. Although it is hard to find a good balance among these limitations and need to be done only after deep investigations which will be the part of our future work.

To gain insight into the issue of daily treatment, it is instructive to investigate the Figs. 8. and 9.

The model has its specific equilibrium belonging to G_B and I_B. Without any external excitation, the states approaching the zero, except $G(t)$ and $I(t)$ which are closing to G_B and I_B, respectively. This is not a limitation, however, this property has to be taken into account. This can be seen on Fig. 8 as well. Without any control input signal, the BG level provided by the model does not slip away. Instead, after the exhaustion of the glucose – when the effect of the food intake is over – the BG level approaches the G_B.

The definition of hypoglycemia and hyperglycemia according to [6], [7], [84] can be found in Table 3.

As it can be seen on Fig. 11. the sensor noise has a determining role in the control, even if we know that the real BG level can be very different. In this research we applied higher additive random noise to simulate the sensor uncertainty. Without applying some kind of filtering it would be difficult

TABLE 3. Definition of hypo- and hyper-glycemia from the applied model point of view.

Hypoglycemia	$G(t) \leq 3.9$ mmol/L (70 [mg/dL])
Hyperglycemia (fasting)	$7 \leq G(t)$ mmol/L (126.126 [mg/dL])
Hyperglycemia (2 hours after meal)	$11.1 \leq G(t)$ mmol/L (200 [mg/dL])

to use the noisy output for control purposes. Thus, by preparing for the errors caused by the sensor, the control solution can be more stable. In this way, the usage of the EKF estimation for control purposes is a reasonable choice as we did in this research – all of these values are in the acceptable range. It should be noted that the controller did not allow the BG level to decrease under 75 [mg/dL] (4, 16 mmol/L), however, it allowed to reach higher glucose values as a consequence that we sought ''soft' control action via the settings of the LMIs. Nevertheless, by the applied soft control action our control solution is able to intervene effectively. Beside it fully avoids the hypoglycemia, it decreases the duration of the hyperglycemic periods and the BG level reached by the model. The duration of the hyperglycemic periods was half as long with treatment as without it and the maximum BG levels are significantly lower both in peaks and average as well. As it is reflected in the blue dots (Fig. 11) the realized BG levels are fairly acceptable – in accordance with the definitions summarized by Table 3.

IX. CONCLUSION AND FURTHER RESEARCH

In this paper, we have proposed a closed loop control solution which was based on the use of different advanced design techniques. TP model transformation, LPV method and LMI optimization have been used in relation to the extended minimal model in control oriented model form for the controller realization. The suggested control framework has been completed with EKF which have provided state estimation and allowed the state feedback kind of control implementation.

We have tested our solution under various circumstances. Namely, we have run long-term simulation (30 days) and we have applied randomized external excitation – CHO intake – in order to investigate the capabilities of the system.

The data reflect that the blood glucose level ($G(t)$ in the model) fluctuated in acceptable range over the simulated time horizon. The mean values belong to the 24 hours periods lie in the tight $133 < G(t) < 143$ [mg/dL] ($7,38 < G(t) < 7,94$ mmol/L) range. Furthermore, the extremes reached by the blood glucose level after higher CHO intake and control action were between 280 [mg/dL] (15.54 mmol/L) and 90 [mg/dL] (4.99 mmol/L), respectively. Therefore, the proposed control solution performed well under the given circumstances.

We have applied additive sensor noise during the simulations which could have heavily influenced the control performance. In this research we only used additive sensor noise, however, in our further research we will investigate

how the performance changes if we add multiplicative noise as well.

By applying Kalman filtering this negative effect can be eliminated. As far as these observations are concerned, it is crucial how to use the measured and filtered (smoothed) blood glucose levels. In daily practice with regular treatment it is the patient's decision how they use the information coming from the measurements to determine the necessary insulin amount. In case of automated insulin administration we have to be sure that the measurements and the filtered values correctly correspond with each other. Sensor decalibration may result in the measurement becoming incorrect which leads to incorrect filtered values as well. In our future work we will investigate how recalibration and estimation possibility can be an automated and implemented in order to avoid mistreatments due to sensor and filter errors.

In our further research we are going to implement other LMIs as well to extend the capabilities of the framework. As we already mentioned these will be connected to the input and output constraints, moreover, we are planning to add higher disturbance rejection properties to the system as well.

ACKNOWLEDGMENT

The authors would like to thank the support of the Hungarian Diabetes Association, the Robotics Special College and the Research, Innovation and Service Center of Óbuda University.

REFERENCES

[1] J. D. Bronzino and D. R. Peterson, *The Biomedical Engineering Handbook*, 4th ed. Boca Raton, FL, USA: CRC Press, 2015.
[2] C. Ionescu, Y. Zhou, and J. A. T. Machado, "Special Issue: Advances in fractional dynamics and control," *J. Vib. Control*, vol. 22, no. 8, pp. 1969–1971, 2016.
[3] A. Haidar, "The artificial pancreas: How closed-loop control is revolutionizing diabetes," *IEEE Control Syst. Mag.*, vol. 36, no. 5, pp. 28–47, Oct. 2016.
[4] L. Kovács, "Linear parameter varying (LPV) based robust control of type-I diabetes driven for real patient data," *Knowl.-Based Syst.*, vol. 122, pp. 199–213, Apr. 2017.
[5] D. A. Drexler, J. Sápi, and L. Kovács, "Modeling of tumor growth incorporating the effects of necrosis and the effect of bevacizumab," *Complexity*, vol. 2017, Nov. 2017, Art. no. 5985031.
[6] *Global Report on Diabetes*, WHO, Geneva, Switzerland, 2016.
[7] *Definition and Diagnosis of Diabetes Mellitus and Intermediate Hyperglycaemia: Report of a WHO/IDF Consultation*, World Health Organization, Geneva, Switzerland, 2006.
[8] T. Ferenci, A. Körner, and L. Kovács, "The interrelationship of HbA1c and real-time continuous glucose monitoring in children with type 1 diabetes," *Diabetes Res. Clin. Pract.*, vol. 108, no. 1, pp. 38–44, 2015.
[9] T. Ferenci, J. Sápi, and L. Kovács, "Modelling tumor growth under angiogenesis in-hibition with mixed-effects models," *Acta Polytechnica Hungarica*, vol. 14, no. 1, pp. 221–234, 2017.
[10] A. Fonyó and E. Ligeti, *Physiology*, (in Hungarian), 3rd ed. Budapest, Hungary: Medicina Press, 2008.
[11] V. Adam, *Medical Biochemistry* (in Hungarian), 4th ed. Budapest, Hungary: Medicina Press, 2006.
[12] A. Bertachi, C. M. Ramkissoon, J. Bondia, and J. Vehí, "Automated blood glucose control in type 1 diabetes: A review of progress and challenges," *Endocrinología, Diabetes y Nutrición (English ed.)*, vol. 65, no. 3, pp. 172–181, 2018.
[13] J. B. Lee, E. Dassau, D. E. Seborg, and F. J. Doyle, "Model-based personalization scheme of an artificial pancreas for type 1 diabetes applications," in *Proc. Amer. Control Conf. (ACC)*, Jun. 2013, pp. 2911–2916.
[14] F. Doyle, E. Dassau, D. Seborg, and J. Lee, "Model-based personalization scheme of an artificial pancreas for type I diabetes applications," Oct. 29, 2015, US Patent 20 150 306 314 A1. [Online]. Available: https://www.google.com/patents/US20150306314
[15] J. E. Pinsker, J. B. Lee, E. Dassau, D. E. Seborg, P. K. Bradley, R. Gondhalekar, W. C. Bevier, L. Huyett, H. C. Zisser, and F. J. Doyle, "Randomized crossover comparison of personalized MPC and PID control algorithms for the artificial pancreas," *Diabetes Care*, vol. 39, no. 7, pp. 1135–1142, 2016.
[16] R. Nimri, H. Yakoob, B. Schoenberg, and E. Dassau, "Closing the loop," *Diabetes Technol. Therapeutics*, vol. 18, no. S1, pp. s27–s41, 2017.
[17] J. Bondia, S. Romero-Vivo, B. Ricarte, and J. L. Diez, "Insulin estimation and prediction: A review of the estimation and prediction of subcutaneous insulin pharmacokinetics in closed-loop glucose control," *IEEE Control Syst. Mag.*, vol. 38, no. 1, pp. 47–66, Feb. 2018.
[18] M. Messori, G. P. Incremona, C. Cobelli, and L. Magni, "Individualized model predictive control for the artificial pancreas: In silico evaluation of closed-loop glucose control," *IEEE Control Syst. Mag.*, vol. 38, no. 1, pp. 86–104, Feb. 2018.
[19] G. Eigner and L. Kovács, "Realization methods of continuous glucose monitoring systems," *Sci. Bull. Politechnica Univ. Timisoara Trans. Autom. Control Comput. Sci.*, vol. 59, no. 73, pp. 175–182, 2014.
[20] T. Donner and S. Sarkar, "Insulin—Pharmacology, therapeutic regimens and principles of intensive insulin therapy," in *Endotext [Internet]*. MDText.com, 2015.
[21] B. W. Bequette, F. Cameron, B. A. Buckingham, D. M. Maahs, and J. Lum, "Overnight hypoglycemia and hyperglycemia mitigation for individuals with type 1 diabetes: How risks can be reduced," *IEEE Control Syst. Mag.*, vol. 38, no. 1, pp. 125–134, Feb. 2018.
[22] L. M. Huyett, E. Dassau, H. C. Zisser, and F. J. Doyle, III, "Glucose sensor dynamics and the artificial pancreas: The impact of lag on sensor measurement and controller performance," *IEEE Control Syst. Mag.*, vol. 38, no. 1, pp. 30–46, Feb. 2018.
[23] A. El Fathi, M. R. Smaoui, V. Gingras, B. Boulet, and A. Haidar, "The artificial pancreas and meal control: An overview of postprandial glucose regulation in type 1 diabetes," *IEEE Control Syst. Mag.*, vol. 38, no. 1, pp. 67–85, Feb. 2018.
[24] K. Turksoy, E. Littlejohn, and A. Cinar, "Multimodule, multivariable artificial pancreas for patients with type 1 diabetes: Regulating glucose concentration under challenging conditions," *IEEE Control Syst. Mag.*, vol. 38, no. 1, pp. 105–124, Feb. 2018.
[25] L. Kovács, "A robust fixed point transformation-based approach for type 1 diabetes control," *Nonlinear Dyn.*, vol. 89, no. 4, pp. 2481–2493, 2017.
[26] J. K. Tar, J. F. Bitó, L. Nádai, and J. A. T. Machado, "Robust fixed point transformations in adaptive control using local basin of attraction," *Acta Polytechnica Hungarica*, vol. 6, no. 1, pp. 21–37, 2009.
[27] P. Colmegna, R. Sánchez-Peña, and R. Gondhalekar, "Linear parameter-varying model to design control laws for an artificial pancreas," *Biomed. Signal Process. Control*, vol. 40, pp. 204–213, Feb. 2018.
[28] I. Nagy, "From exploring to optimal path planning: Considering error of navigation in multi-agent mobile robot domain," *Acta Polytechnica Hungarica*, vol. 11, no. 6, pp. 39–55, 2014.
[29] P. Szalay, G. Eigner, and L. Kovács, "Linear matrix inequality-based robust controller design for type-1 diabetes model," in *Proc. 19th World Congr. Int. Fed. Autom. Control (IFAC)*, 2014, pp. 9247–9252.
[30] P. Palumbo, S. Ditlevsen, A. Bertuzzi, and A. de Gaetano, "Mathematical modeling of the glucose–insulin system: A review," *Math. Biosci.*, vol. 244, no. 2, pp. 69–81, 2013.
[31] G. Eigner, "Novel LPV-based control approach for nonlinear physiological systems," *Acta Polytechnica Hungarica*, vol. 14, no. 1, pp. 45–61, 2017.
[32] D. Wu, D. Cao, T. Wang, Y. Fang, and J. Fei, "Adaptive neural LMI-based H-infinity control for MEMS gyroscope," *IEEE Access*, vol. 4, pp. 6624–6630, 2016.
[33] K. Tanaka and H. Wang, *Fuzzy Control Systems Design and Analysis: A Linear Matrix Inequality Approach*, 1st ed. Chichester, U.K.: Wiley, 2001.
[34] P. Baranyi, Y. Yam, and P. Várlaki, *Tensor Product Model Transformation in Polytopic Model-Based Control* (Automation and Control Engineering), 1st ed. Boca Raton, FL, USA: CRC Press, 2013.
[35] J. Kuti, P. Galambos, and P. Baranyi, "Minimal volume simplex (MVS) polytopic model generation and manipulation methodology for TP model transformation," *Asian J. Control*, vol. 19, no. 1, pp. 289–301, 2017.

[36] Á. Takács, T. Haidegger, P. Galambos, J. Kuti, and I. J. Rudas, "Nonlinear soft tissue mechanics based on polytopic tensor product modeling," in *Proc. IEEE 14th Int. Symp. Appl. Mach. Intell. Inform. (SAMI)*, Jan. 2016, pp. 211–215.

[37] V. C. da Silva Campos, V. A. B. Tôrres, and R. M. Palhares, "Revisiting the TP model transformation: Interpolation and rule reduction," *Asian J. Control*, vol. 17, no. 2, pp. 392–401, 2015.

[38] J. Pan and L. Lu, "TP model transformation via sequentially truncated higher-order singular value decomposition," *Asian J. Control*, vol. 17, no. 2, pp. 467–475, 2015.

[39] T. T. Wang, W. F. Xie, G. D. Liu, and Y. M. Zhao, "Quasi-min-max model predictive control for image-based visual servoing with tensor product model transformation," *Asian J. Control*, vol. 17, no. 2, pp. 402–416, Mar. 2015.

[40] G. Zhao, H. Li, and Z. Song, "Tensor product model transformation based decoupled terminal sliding mode control," *Int. J. Syst. Sci.*, vol. 47, no. 8, pp. 1791–1803, 2016.

[41] R.-E. Precup, E. M. Petriu, M.-B. Rădac, S. Preitl, L.-O. Fedorovici, and C.-A. Dragoş, "Cascade control system-based cost effective combination of tensor product model transformation and fuzzy control," *Asian J. Control*, vol. 17, no. 2, pp. 381–391, 2015.

[42] G. Zhao, D. Wang, and Z. Song, "A novel tensor product model transformation-based adaptive variable universe of discourse controller," *J. Franklin Inst.*, vol. 353, no. 17, pp. 4471–4499, 2016.

[43] X. Liu, Y. Yu, Z. Li, H. H. C. Iu, and T. Fernando, "An efficient algorithm for optimally reshaping the TP model transformation," *IEEE Trans. Circuits Syst., II, Exp. Briefs*, vol. 64, no. 10, pp. 1187–1191, Oct. 2017.

[44] P. Baranyi, *TP-Model Transformation-Based-Control Design Frameworks*. Cham, Switzerland: Springer, 2016.

[45] A. Szollosi and P. Baranyi, "Influence of the tensor product model representation of qLPV models on the feasibility of linear matrix inequality based stability analysis," *Asian J. Control*, vol. 20, no. 1, pp. 531–547, 2018.

[46] F. Chee and T. Fernando, *Closed-Loop Control of Blood Glucose*. Berlin, Germany: Springer, 2007.

[47] R. Hovorka, V. Canonico, L. J. Chassin, U. Haueter, M. Massi-Benedetti, M. O. Federici, T. R. Pieber, H. C. Schaller, L. Schaupp, T. Vering, and W. M. Wilinska, "Nonlinear model predictive control of glucose concentration in subjects with type 1 diabetes," *Physiolog. Meas.*, vol. 25, no. 4, pp. 905–920, 2004.

[48] D. Boiroux, M. Hagdrup, Z. Mahmoudi, K. Poulsen, H. Madsen, and J. B. Jørgensen, "An ensemble nonlinear model predictive control algorithm in an artificial pancreas for people with type 1 diabetes," in *Proc. Eur. Control Conf. (ECC)*, Jun./Jul. 2016, pp. 2115–2120.

[49] D. Boiroux, A. K. Duun-Henriksen, S. Schmidt, K. Nørgaard, N. K. Poulsen, H. Madsen, and J. B. Jørgensen, "Adaptive control in an artificial pancreas for people with type 1 diabetes," *Control Eng. Pract.*, vol. 58, pp. 332–342, Jan. 2017.

[50] K. Turksoy and A. Cinar, "Adaptive control of artificial pancreas systems—A review," *J. Healthcare Eng.*, vol. 5, no. 1, pp. 1–22, 2014.

[51] R. Hovorka, F. Shojaee-Moradie, P. V. Carroll, L. J. Chassin, I. J. Gowrie, N. C. Jackson, R. S. Tudor, A. M. Umpleby, and R. H. Jones, "Partitioning glucose distribution/transport, disposal, and endogenous production during IVGTT," *Amer. J. Physiol.-Endocrinol. Metabolism*, vol. 282, no. 5, pp. E992–E1007, 2002.

[52] D. Boiroux, V. Bátora, M. Hagdrup, S. L. Wendt, N. K. Poulsen, H. Madsen, and J. B. Jørgensen, "Adaptive model predictive control for a dual-hormone artificial pancreas," *J. Process Control*, vol. 68, pp. 105–117, Aug. 2018.

[53] A. P. White, G. Zhu, and J. Choi, *Linear Parameter-Varying Control for Engineering Applications*, 1st ed. London, U.K.: Springer, 2013.

[54] M. Chilali and P. Gahinet, "H_∞ design with pole placement constraints: An LMI approach," *IEEE Trans. Autom. Control*, vol. 41, no. 3, pp. 358–367, Mar. 1996.

[55] O. Sename, P. Gáspár, and J. Bokor, *Robust Control and Linear Parameter Varying Approaches: Application to Vehicle Dynamics* (Lecture Notes in Control and Information Sciences), vol. 437. Berlin, Germany: Springer-Verlag, 2013.

[56] W. Levine, *The Control Engineering Handbook*, 2nd ed. Boca Raton, FL, USA: CRC Press, 2011.

[57] P. Baranyi, "TP model transformation as a way to LMI-based controller design," *IEEE Trans. Ind. Electron.*, vol. 51, no. 2, pp. 387–400, Apr. 2004.

[58] P. Galambos and P. Baranyi, "TP^T model transformation: A systematic modelling framework to handle internal time delays in control systems," *Asian J. Control*, vol. 17, no. 2, pp. 486–496, 2015.

[59] J. Kuti, P. Galambos, P. Baranyi, and P. Várlaki, "A hands-on demonstration of control performance optimization using tensor product model transformation and convex hull manipulation," in *Proc. IEEE Int. Conf. Syst., Man, Cybern. (SMC)*, Oct. 2015, pp. 2609–2614.

[60] M. de Berg, O. Cheong, M. van Kreveld, and M. Overmars, *Computational Geometry: Algorithms and Applications*, 3rd ed. Heidelberg, Germany: Springer, 2008.

[61] B. Takarics and P. Baranyi, "Friction compensation in TP model form—Aeroelastic wing as an example system," *Acta Polytechnica Hungarica*, vol. 12, no. 4, pp. 127–145, 2015.

[62] L.-E. Hedrea, C.-A. Bojan-Dragos, R.-E. Precup, R.-C. Roman, E. M. Petriu, and C. Hedrea, "Tensor product-based model transformation for position control of magnetic levitation systems," in *Proc. IEEE 26th Int. Symp. Ind. Electron. (ISIE)*, Jun. 2017, pp. 1141–1146.

[63] MTA SZTAKI. (2016). *TPtool—Tensor Product MATLAB Toolbox*. [Online]. Available: http://tptool.sztaki.hu

[64] C. Scherer and S. Weiland, *Linear Matrix Inequalities in Control*, 2nd ed. Delft, The Netherlands: Delft Univ. of Technology, 1999.

[65] G. Duan and H. Yu, *LMIs in Control Systems: Analysis, Design and Applications*, 1st ed. Boca Raton, FL, USA: CRC Press, 2013.

[66] M. Chilali, P. Gahinet, and P. Apkarian, "Robust pole placement in LMI regions," *IEEE Trans. Autom. Control*, vol. 44, no. 12, pp. 2257–2270, Dec. 1999.

[67] W. El Messoussi, O. Pagès, and A. El Hajjaji, "Robust pole placement for fuzzy models with parametric uncertainties: An LMI approach," in *Proc. EUSFLAT Conf.*, 2005, pp. 810–815.

[68] G. Balas, R. Chiang, A. Packard, and M. Safonov, *Robust Control Toolbox Getting Started Guide*. Natick, MA, USA: Mathworks, 2018.

[69] M. H. Bouazizi, A. Kochbati, and M. Ksouri, "LPV control with observed state feedback and dynamic output feedback," in *Proc. Amer. Control Conf.*, vol. 5, Jun. 2001, pp. 3908–3913.

[70] M. H. Bouazizi, A. Kochbati, and M. Ksouri, "LPV control with observer and dynamic compensator," in *Proc. Eur. Control Conf. (ECC)*, Sep. 2001, pp. 444–450.

[71] MOSEK ApS. (2015). *The MOSEK Optimization Toolbox for MATLAB Manual. Version 7.1 (Revision 28)*. [Online]. Available: http://docs.mosek.com/7.1/toolbox/index.html

[72] J. Löfberg, "YALMIP: A toolbox for modeling and optimization in MATLAB," in *Proc. CACSD Conf.*, Taipei, Taiwan, Sep. 2004, pp. 284–289.

[73] K. Ogata and Y. Yang, *Modern Control Engineering*, vol. 4. New Delhi, India: Prentice-Hall, 2002.

[74] A. Facchinetti, S. Del Favero, G. Sparacino, J. R. Castle, W. K. Ward, and C. Cobelli, "Modeling the glucose sensor error," *IEEE Trans. Biomed. Eng.*, vol. 61, no. 3, pp. 620–629, Mar. 2014.

[75] M. S. Grewal and A. P. Andrews, *Kalman Filtering: Theory and Practice Using MATLAB*, 3rd ed. Chichester, U.K.: Wiley, 2008.

[76] J. Hartikainen, A. Solin, and S. Särkkä, *Optimal Filtering With Kalman Filters and Smoothers a Manual for the MATLAB Toolbox EKF/UKF*, version 1.3 ed., 2011.

[77] *MATLAB, Control System Toolbox Getting Started Guide*, MathWorks, Natick, MA, USA, 2018.

[78] T. M. S. Wolever, S. Hamad, J.-L. Chiasson, R. G. Josse, L. A. Leiter, N. W. Rodger, S. A. Ross, and E. A. Ryan, "Day-to-day consistency in amount and source of carbohydrate intake associated with improved blood glucose control in type 1 diabetes," *J. Amer. College Nutrition*, vol. 18, no. 3, pp. 242–247, 1999.

[79] J. P. Bantle, J. Wylie-Rosett, A. L. Albright, C. M. Apovian, N. G. Clark, M. J. Franz, B. J. Hoogwerf, A. H. Lichtenstein, E. Mayer-Davis, A. D. Mooradian, and M. L. Wheeler, "Nutrition recommendations and interventions for diabetes: A position statement of the american diabetes association," *Diabetes Care*, vol. 31, no. Suppl 1, pp. S61–S78, 2008.

[80] U.S. Department of Health and Human Services and U.S. Department of Agriculture. (2015). *2015–2020 Dietary Guidelines for Americans*. [Online]. Available: https://health.gov/dietaryguidelines/2015/guidelines/

[81] A. B. Evert, J. L. Boucher, M. Cypress, S. A. Dunbar, M. J. Franz, E. J. Mayer-Davis, J. J. Neumiller, R. Nwankwo, C. L. Verdi, and P. Urbanski, "Nutrition therapy recommendations for the management of adults with diabetes," *Diabetes care*, vol. 37, pp. S120–S143, Jan. 2014.

[82] R. Burns, *Advanced Control Engineering*, 1st ed. Oxford, U.K.: Butterworth-Heinemann, 2001.

[83] L. Magni, D. M. Raimondo, C. D. Man, M. Breton, S. Patek, G. De Nicolao, C. Cobelli, and B. P. Kovatchev, "Evaluating the efficacy of closed-loop glucose regulation via control-variability grid analysis," *J. Diabetes Sci. Technol.*, vol. 2, no. 4, pp. 630–635, 2008.
[84] American Diabetes Association, "Diagnosis and classification of diabetes mellitus," *Diabetes care*, vol. 37, pp. S81–S90, Jan. 2014.

LEVENTE KOVÁCS (M'09–SM'17) received the M.Sc. degree in electrical engineering from Politehnica University Timisoara, Romania, in 2000, the M.Sc. degree in biomedical engineering and the Ph.D. degree from the Budapest University of Technology and Economics, Hungary, in 2008 and 2011, respectively, and the Habilitation degree (Hons.) from Óbuda University, in 2013. He was János Bolyai Research Fellow of the Hungarian Academy of Sciences, from 2012 to 2015. He is currently the Rector of Óbuda University and the Head of the Physiological Controls Research Center. His current research interests include modern control theory and physiological controls. He has published more than 390 articles in international journals and refereed international conference articles in the above areas, accumulating an impact factor of over 30 and h-index of 21. Dr. Kovács has been a member of the IFAC TC 8.2 Biological and Medical Systems, since 2010, and the Hungarian Diabetes Association, since 2010. He has been an IEEE EMBS and the IEEE SMC Society Member, since 2012, and an IEEE CSS Society Member, since 2013. He was a recipient of the highly prestigious ERC StG Grant of the European Union, in 2015. At the IEEE Hungary Section level, he was a Membership Development Officer, from 2010 to 2016. He was the Vice-Chair, from 2013 to 2016. He has been the Chair of the IEEE Hungary Section, since 2017. Since 2015, he has been elected as the Chair of the IEEE SMC Hungary Chapter and in 2018, he established the IEEE CSS Hungary Chapter.

GYÖRGY EIGNER (GSM'13–M'17–SM'19) received the B.Sc. degree in mechatronical engineering from Donát Bánki Faculty of Mechanical and Safety Engineering, Óbuda University, in 2011, the M.Sc. degree in biomedical engineering from the Budapest University of Technology and Economics, in 2013, and the Ph.D. degree from Óbuda University, in 2017, where he is currently an Assistant Professor with the John von Neumann Faculty of Informatics. He is also the Deputy Head of the Biomatics and Artificial Intelligent Institution. His current research interests include the application of advanced control methods in physiological relations. He has published more than 70 scientific articles in the above area. His h-index is seven. He is a member of the Board of Governors of the IEEE System, Man, and Cybernetics Society, a Co-Chair of the Computational Cybernetics Technical Committee, a Chair of the SMCS Young Professional Subcommittee of SMCS, and a member of the Robotics Special College, Óbuda University.

MÁTÉ SIKET received the B.Sc. degree in mechatronics and the M.Sc. degree in biomedical engineering from the Budapest University of Technology and Economics. He is currently pursuing the Ph.D. degree with Óbuda University. His current research interests include controlling and modeling of physiological systems and the developments of non-contact measurements regarding vital physiological signs.

LÁSZLÓ BARKAI received the M.D. degree from the University of Debrecen, in 1982. He received the degrees in pediatry, pediatric pulmonology, health care management, and diabetology, in 1986, 1995, 1996, and 1997, respectively. He is currently a Full Professor with Pavol Jozef Šafárik University, Košice, Slovakia, the University of Miskolc, and the University of Debrecen, Hungary. He is also a Clinician with the Markhot Ferenc Teaching Hospital and Clinic in Eger, Hungary. He is currently the Vice-President (as Past-President) of the Hungarian Diabetes Association. His current research interests include epidemiology, treatment, care, and complications of type 1 and type 2 diabetes in childhood; and cardiometabolic risk factors and metabolic syndrome in children and adolescents. He published more than 175 scientific articles in these areas. His cumulative impact factor is over 80, h-index is 17. He is supervising the research work of several Ph.D. students in the field of childhood diabetes and its complications. He received the Heténi Géza and Magyar Imre Awards from the Hungarian Diabetes Association, the Batthyány-Strattmann László Award from the Ministry of Health, and the Scientific Excellence Award and the Markhot Award from the Markhot Ferenc Teaching Hospital and Clinic and Miskolc Regional Committee of the Hungarian Academy of Sciences. He is the Co-leader of the Hungarian Artificial Pancreas working group established, in 2010.